Effect of treating activated carbon derived from date pits with H_2SO_4 on the adsorption of methylene blue dye molecules: kinetic, equilibrium and thermodynamic studies

Abdelkader Guemgam[1*], Abdelali Gherbia[2], Boulanouar Bakchiche[3], Hadjira Guenane[3]

[1] Laboratory of Process Engineering, Amar Telidji University of Laghouat, BP 37G, Laghouat 03000, Algeria.

[2] Department of Technical Sciences, Amar Telidji University of Laghouat, BP 37G, Laghouat 03000, Algeria.

[3] Laboratory of Biological and Agricultural Sciences (LBAS), Amar Telidji University of Laghouat, BP 37G, Laghouat 03000, Algeria.

[*]Email: aek.guemgam@lagh-univ.dz, tel: +213 668646329

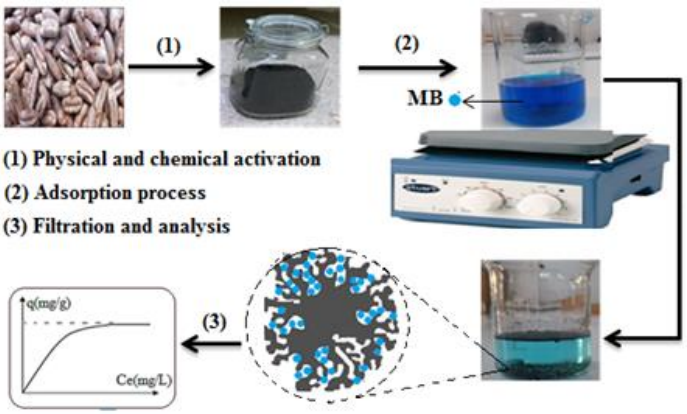

Graphical abstract

ABSTRACT

In this work, untreated activated carbon (UDP-AC) and activated carbon chemically treated with H_2SO_4 (TDP-AC) were successfully synthesized from date pits, a solid waste material. Characterization was performed on both UDP-AC and TDP-AC, and both samples were used to adsorb methylene blue (MB) dye from an aqueous solution. BET and BJH analyses were used to determine the surface area and pore size distribution. FTIR analysis confirmed the involvement of functional groups on the surfaces in the MB adsorption process. Scanning electron microscope (SEM-EDX) examination revealed that the adsorbents' surfaces are heterogeneous and irregularly rough, with varying porosity, making them suitable for contaminant removal. The effects of several operating parameters, including adsorbent dose (0.05–0.5 g in 100 mL), initial pH (2–10), contact time (0–180 min), initial MB concentration (50–500 mg L^{-1}), and temperature (298–328 K), on MB removal were studied using batch mode operation. Adsorption kinetic data were best described by the pseudo-second-order model ($R^2 = 0.99$). The adsorption isotherm was well fitted by the Langmuir model, with maximum monolayer adsorption capacities of 270.27 mg g^{-1} and 327.86 mg g^{-1} at 25°C for UDP-AC and TDP-AC, respectively. Thermodynamic investigations indicated that the adsorption process is physical in nature, increases system randomness, and is feasible and spontaneous. These results provide evidence that activated carbon derived from date pits can serve as an inexpensive, eco-friendly, and efficient adsorbent for the removal of MB dye from wastewater.

Keywords: Adsorption, Agricultural Residues, Activated Carbon, Chemical Activation, Methylene Blue.

1. Introduction

Water pollution poses a major environmental challenge, primarily due to human activities such as the discharge of industrial effluents, the excessive use of agricultural pesticides and fertilizers, and improper waste disposal methods. The release of polluted water can lead to the destruction of aquatic ecosystems, pose risks to human health, threaten agricultural sustainability, and contribute to the deterioration of water quality (Lu et al., 2021) (Yeliz Ozudogru & Ecem Tekne, 2023).

The textile industry consumes a large quantity of synthetic dyes, accounting for approximately 75% (6×10^2 tons) of global synthetic dye production, along with a significant volume of water. It has been reported that approximately 125 to 200 L of water is required per kilogram of textile during the dyeing process. This sector subsequently discharges large volumes of wastewater containing dyes and other toxic and harmful chemicals such as salts, metals, carriers, and detergents. It is estimated that each year, 10^2 tons of dyes from textile industries are released into rivers, which has become a major environmental concern. Therefore, wastewater generated by textile factories must be treated before being discharged into the environment. Additionally, beyond water pollution, dyeing processes contribute to more than 3.3×10^9 metric tons of greenhouse gas emissions annually (Okoniewska, 2021) (Chopra & Singh, 2020) (Vojnović et al., 2022) (Pizzicato et al., 2023).

The presence of dye-laden liquid waste in aquatic environments prevents sunlight penetration, thereby inhibiting photosynthesis in many aquatic plants, increasing pH levels, and ultimately harming aquatic organisms. In response to these threats and to protect the environment, several methods have been employed to remove dye contaminants from water, including biological treatment, photocatalytic reduction, electrochemical processes, distillation, coagulation and flocculation, precipitation, adsorption, membrane separation, and ozonation (Okoniewska, 2021) (Sen, 2023) (Soltani et al., 2021).

However, some of these processes are not entirely satisfactory due to disadvantages such as low efficiency, high capital costs, and excessive consumption of chemicals and energy. In contrast, adsorption is considered one of the most promising techniques. It has gained significant interest due

to its numerous advantages, including cost-effectiveness, simplicity, ease of operation, minimal generation of harmful by-products, and high efficiency in treating a wide range of pollutants. Furthermore, the adsorption capacity can be optimized through physical and chemical activation, and a variety of adsorbents are now available for different applications (Wijaya et al., 2023) (Somsesta et al., 2020) (Mechi et al., 2019) (Razali et al., 2022) .

Activated carbon is widely used in various industrial processes due to its high adsorption capacity, selectivity, effectiveness in removing both organic and inorganic contaminants, high mechanical strength, large surface area, porosity, and affordability, particularly when derived from locally available renewable natural sources such as agricultural solid waste (Jawad et al., 2018).

Chemical activation is a widely used method for producing activated carbon with high porosity and surface area. This process involves treating the carbon precursor with chemical agents such as acids (H_2SO_4, HCl, H_3PO_4), bases (KOH, NaOH), or salts ($ZnCl_2$, $FeCl_3$) before carbonization. Acid activation enhances porosity and introduces functional groups that improve adsorption properties, with phosphoric acid (H_3PO_4) (Fito et al., 2023) (Jabar et al., 2022), being particularly effective in developing mesopores. Alkali activation, especially with potassium hydroxide (KOH) (Yasin et al., 2007), creates a highly microporous structure with a large surface area, making it ideal for gas adsorption. Salt activation, commonly using zinc chloride ($ZnCl_2$) (Gao et al., 2013), helps develop a well-defined pore structure with a balance of micro- and meso-porosity.

Among these activating agents, sulfuric acid (H_2SO_4) is a highly reactive chemical activator capable of dissolving various organic compounds (such as carbohydrates and other organic matter), as well as minerals and impurities from AC precursors (Mousavi et al., 2022) (Al-Qodah & Shawabkah, 2009). Its use is cost-effective and contributes to the formation of medium to large porosity on the AC surface (Togibasa et al., 2023) (Olivares-Marín et al., 2012) .In this study, sulfuric acid activation was chosen to enhance the textural properties of activated carbon derived from local date pits, optimizing its efficiency in the adsorption of MB.

In Algeria, dates are among the most significant agricultural products, produced in large quantities. The industrial processing of dates generates substantial amounts of date pits, which are typically burned or discarded as waste. Consequently, it is essential to explore low-cost applications for these residues to create value-added products while addressing environmental concerns. This approach not only reduces waste but also promotes the circular economy by repurposing biomass for pollution control. Given the abundance and renewability of date pits, their conversion into activated carbon provides an eco-friendly and cost-effective alternative to conventional adsorbents, aligning with global efforts toward sustainable resource utilization.

Therefore, this study aims to investigate the effectiveness of both untreated activated carbon (UDP-AC) and chemically treated activated carbon (TDP-AC) with sulfuric acid (H_2SO_4), derived from date pits as solid waste, for the removal of methylene blue (MB) dye from aqueous solutions. Various characterization techniques, including X-ray diffraction (XRD), Fourier-transform infrared spectroscopy (FTIR), thermogravimetric analysis (TGA), scanning electron microscopy with energy-dispersive X-ray spectroscopy (SEM-EDX), and surface charge analysis, were employed to examine the surface structure of both samples before and after the adsorption process. Batch adsorption experiments were conducted to assess the influence of key factors on MB adsorption capacity, including contact time (0–180 min), initial MB concentration (50–500 mg L^{-1}), initial pH (2–10), and adsorbent dosage (0.05–0.5 g), followed by a thermodynamic study.

2. Materials and methods

2.1. Adsorbate

Methylene blue (MB) (98.5% purity, chemical formula: $C_{16}H_{18}N_3SCl$, molecular weight = 319.85 g mol^{-1}) was selected as the model cationic dye in this study. Its chemical structure is shown in Figure 1. MB is highly soluble in water (43.6 g L^{-1}) and is widely used in various applications, particularly in the textile industry. However, it is classified as a hazardous substance due to its potential harmful effects on humans, animals, and the environment. A stock solution of MB (500 mg L^{-1}) was prepared by dissolving 0.5 g of MB powder in 1 L of distilled water. Experimental solutions were obtained by

diluting the stock solution to the desired concentrations. The initial pH of the experimental solutions was adjusted using either hydrochloric acid (HCl, 0.1 M) or sodium hydroxide (NaOH, 0.1 M), both supplied by Sigma-Aldrich. The concentration of MB solutions was determined at a maximum wavelength (λ_{max}) of 664 nm using UV-Visible spectrophotometry (I. Khan et al., 2022) (Rafatullah et al., 2010).

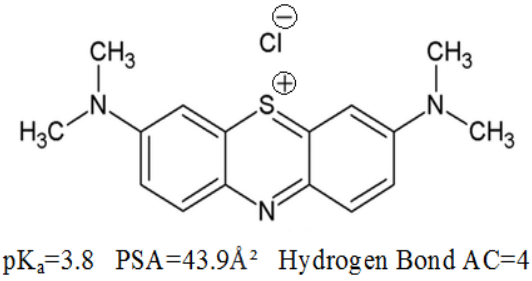

pK_a=3.8 PSA=43.9Å² Hydrogen Bond AC=4

Figure 1. Chemical structure of methylene blue MB.

2.2 Preparation of the adsorbents

Figure 2 represents the preparation of adsorbent materials from date pits. The date pits as a solid waste were obtained from southern Algeria, initially, the sample was washed with tap water several times in order to remove soluble impurities, then with distilled water, dried in an oven at a temperature of 105 °C for 24 h, then crushed and sieved, followed by physically activation using pyrolysis in a muffle furnace (Nabertherm P330. Germany) at a rate of 5°C min^{-1} until reaching 600 °C, it was maintained for 2 hours, the obtained sample was grounded and sieved to obtain a powder with diameter ≤ 0.315 mm, it was then stored in an airtight bottle, ready to use as (UDP-AC). A part of UDP-AC was subjected to chemical activation by adding 50 g of UDP-AC to 250 mL of H_2SO_4 (1M) sulfuric acid solution, the mixture was stirred for 24 h, then washed with distilled water and dried in an oven at 105 °C for 24 h. Relatively dilute acids tend to dissociate more than concentrated acids, leading to the expectation that adsorbents activated with dilute acids will have a higher density of surface functional groups (Bozbeyoglu et al., 2020) (Cox et al., 1999). After that, the obtained sample was then stored in an airtight bottle, ready for use as (TDP-AC).

2.3 Characterization of UDP-AC and TDP-AC

The Brunauer, Emmett, and Teller (BET) surface area and the pore size distributions of the adsorbents UDP-AC and TDP-AC were calculated from Nitrogen adsorption/desorption isotherms at T = -196.271 °C, using micromeritics ASAP 2020 Plus Version 2.00, USA. pH_{PZC} points zero charge of UDP-AC and TDP-AC adsorbents were measured by adding 0.2 g of UDP-AC or TDP-AC to a set of Erlenmeyer flask containing 100 ml of KNO_3 (0.1M) as background electrolyte, the solutions were adjusted at different pH from 1 to 12 by the addition of 0.1 mol L^{-1} of NaOH or HNO_3, the flasks were stirred at 100 rpm for 48h to reach equilibrium. The functional groups present on UDP-AC and TDP-AC surfaces before and after the MB adsorption process of were obtained using Fourier transform infrared spectrophotometer (FTIR, INVENIO-X) in the region of 400–4000 Cm^{-1}. The Surface morphology of adsorbents UDP-AC and TDP-AC were studied using scanning electron microscopy (Scios 2 DualBeam / FIB-SEM-EDX system) at working distance (6.5-6.7) mm, an accelerating voltage of 5.0 kV and at magnification of 3500X. X Ray Diffraction XRD patterns of TDP-AC were obtained on x-ray diffractometer (Empyrean X-ray Diffraction System) and the thermogravimetric analysis TGA/TDA of UAC was performed in a thermogravimetric analyzer (Setaram Labsys Evo). The heating rate was fixed at 10 °C min^{-1} to 1000 °C.

2.4 Batch adsorption experiments

Adsorption experiments were carried out in a batch system (Orbital laboratory shaker ST 30-Nuve-Digital/Benchtop) using a series of flasks containing 100 mL of MB, stirring speed 150 rpm for 180 min, an initial MB concentration of (100 mg L^{-1}) and room temperature (25 ±1) °C as shown in figure 2. The effect of adsorbent dosage was performed in the range (0.05-0.5g) and pH 6. The effect of initial pH was evaluated in the range of (2-10), with (0.05 g) of adsorbent mass. The interval time (0-180min) was chosen to study the kinetic of MB adsorption using 0.05 g of adsorbent and pH of 6. The isotherm study was conducted at variable MB concentration C_0 (50-500 mg L^{-1}), at pH of 6 and adsorbent mass of 0.05 g. The concentration of MB in solution at equilibrium was measured by UV-visible spectrophotometer (U-2000 model) at λ = 664 nm.

The adsorption capacity at equilibrium q_e (mg g^{-1}), at time t, q_t (mg g^{-1}) and the percentage removal R (%) were calculated by the following equations (Gherbia et al., 2019):

$$q_e = \frac{(C_0 - C_e)}{m} V \quad (1)$$

$$q_t = \frac{(C_0 - C_t)}{m} V \quad (2)$$

$$R\,\% = \frac{(C_0 - C_e)}{C_0} 100 \quad (3)$$

Where C_0, C_e and C_t (mg L^{-1}) are the concentration of MB solution at initial, equilibrium and at time t, respectively. m (g) is the mass of the adsorbent and V (L) is the volume of MB solution.

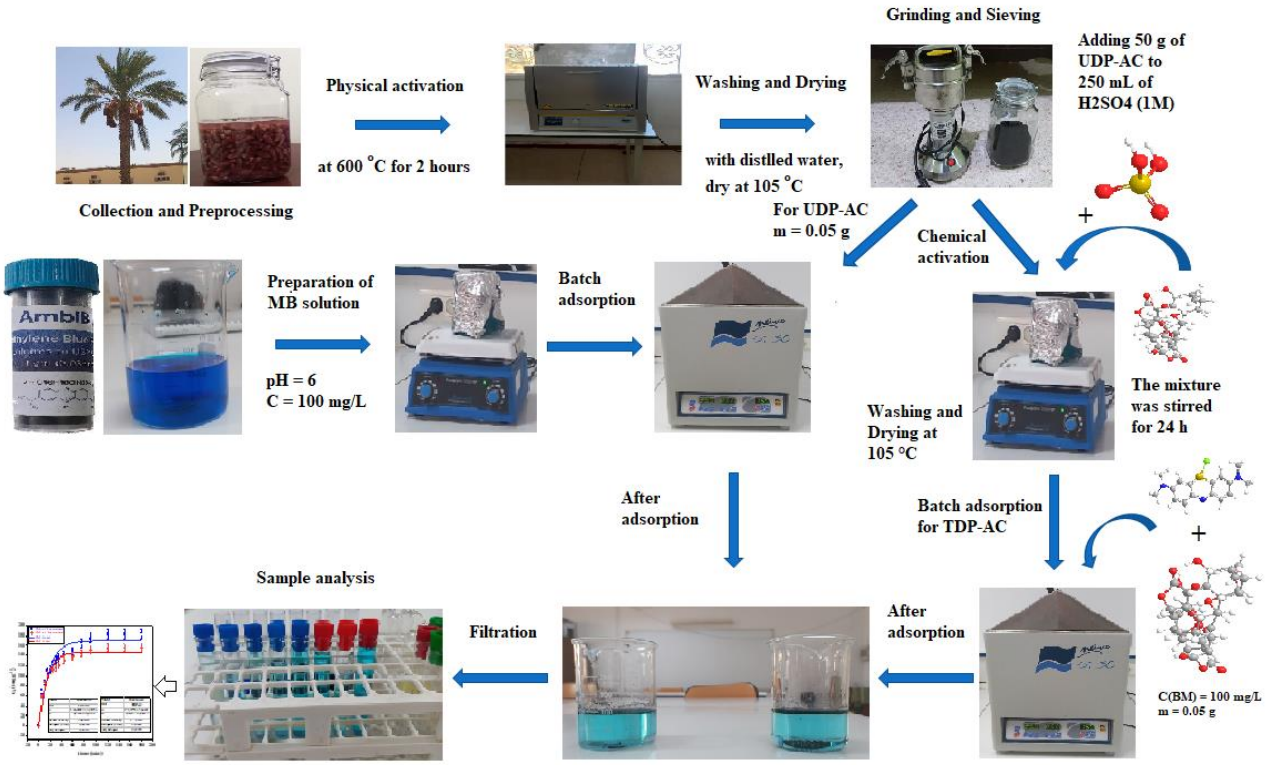

Figure 2. Stages of adsorbent material preparation and Batch adsorption process (C_0 = 100 mg L^{-1}, pH 6, t = 120 min).

3. Results and discussion

3.1. Characterization of UDP-AC and TDP-AC

The specific surface area and pore size distribution of solids are of interest in many industries and processes that involve surfaces interacting with gases or liquids. Figures 3 (a, b, c) represent a nitrogen adsorption isotherm for UDP-AC and TDP-AC samples, the linear form of the BET model was applied to determine the specific surface area of the samples and the pore size distributions for UDP-

AC and TDP-AC samples were calculated by the BJH (Barrett, Joyner and Halenda) method. The samples UDP-AC and TDP-AC have a specific surface area of around 230.3 and 286.36 m^2 g^{-1} with a pore size distribution around 3.356 and 4.059 nm, respectively. Indicating the presence of mesopores (2–50 nm), also, the activation process with H_2SO_4 contributed to the increase in the specific surface area and pore size distribution of both adsorbents (Ahmad et al., 2020).

The point of zero charge (pH_{pzc}) is a critical parameter for understanding the surface charge of adsorbents at different pH levels, which in turn influences the adsorption mechanism. The pH_{pzc} values of UDP-AC and TDP-AC were determined by plotting ΔpH = (pHi – pHf) versus the initial pHi, as shown in Figure 5(a). The pH_{pzc} values were found to be 6.37 for UDP-AC and 5.78 for TDP-AC. These values indicate the acidic nature of both adsorbents, suggesting the presence of acidic functional groups on their surfaces. The lower pH_{pzc} of TDP-AC compared to UDP-AC confirms that sulfuric acid (H_2SO_4) treatment increased the acidity of the activated carbon. The pH_{pzc} value is strongly influenced by the chemical activation process. When the solution pH is lower than the pH_{pzc}, the adsorbent surface becomes positively charged, favoring the adsorption of negatively charged species. When the solution pH is higher than the pH_{pzc}, the adsorbent surface becomes negatively charged, favoring the adsorption of positively charged species such as MB.

Figure 6 illustrates the FTIR spectrum for TDP-AC and UDP-AC before and after adsorption of MB, respectively. Before adsorption of MB, the broad bands at around 3417.34 and 3433.12 cm^{-1} usually attributed to hydroxyl groups O–H stretching vibrations of adsorbed water on carbon, phenols, carboxylic acids or alcohols. The peaks at 2923.94 and 2920.08 cm^{-1} are assigned to the aliphatic C–H stretching (=CH–, $–CH_3$ and $–CH_2–$ groups). The bands observed at 1595.05 and 1602.76 cm^{-1} are related to C=C vibrations in aromatic rings. Finally, the bands at 1164.94 and 1176.52 cm^{-1} are attributed to C–O or C–O–C stretching of esters, ethers, phenols, alcohols and acids groups. After the adsorption of MB on TDP-AC and UDP-AC respectively, the broad bands of O–H stretching vibrations were shifted to 3409.98 and 3419.62 cm^{-1}, the peaks of aliphatic C–H stretching were shifted to 2925.87 and 2922.01 cm^{-1}, probably formation of hydrogen bonds, the bands of C=C

vibrations were shifted to 1600.84 and 1596.98 cm^{-1}, can be attributed to the interaction in C=C aromatic adsorbent with the aromatic rings of MB dye molecules. the bands of C–O or C–O–C stretching were shifted to 1161.09 and 1157.23 cm^{-1}, respectively. The shifts reflect the possibility of the involvement of these functional groups present on the surfaces in MB adsorption process by n -π interactions (Harabi et al., 2024)(Tran et al., 2017). Furthermore, EDX analysis confirmed the presence of sulfonic acid (–SO_3H) groups on TDP-AC, particularly in the 1000–1350 cm^{-1} region of the FTIR spectrum. The presence of these groups, introduced by H_2SO_4 activation, enhances the adsorption capacity of TDP-AC (Jawad et al., 2018).

The thermal stability of date pits solid waste was studied by thermal gravimetric analysis TGA and the resulting curves of the weight loss and the thermogravimetric derivative analysis DTG are shown in Figure 7. DTA curve showed three peaks resultant to three weight losses. The first stage from 26.71°C to approximately 175.37°C corresponds to a weight loss of 6.626 (%) due to the moisture present on the surface and the evaporation water (dehydration). The second stage in the temperature range from 175.47°C to 337.42°C, corresponding to a significant weight loss of about 52.356 (%) due to the degradation of hemicellulose and cellulose constituents. The last stage for temperatures ranging from 337.42°C to 500°C presents a mass loss of 23.297 (%) was attributed to the decomposition of lignin. Above 500°C, represents the residues formed after the decomposition of lignocellulose (Alghamdi & El Mannoubi, 2021)(Edokpayi et al., 2019)(Akköz & Coşkun, 2024).

Figure 4 illustrates the XRD patterns for TDP-AC and MB loaded TDP-AC. The broad diffraction peak seen at 2θ = 20.45° characterizes the graphite crystallinity in both samples. The sample TDP-AC had an amorphous structure, helps for the easy diffusion of MB dye molecules to its surface and would cause an effective MB dye molecules removal, after MB adsorption a new peak was formed at 2θ = 78.32° was observed which was due to the interactions between the functional groups of the adsorbent TDP-AC and adsorbate MB dye molecules. It is also considered evidence of the binding of methylene blue on TDP-AC (Sarkar Phyllis et al., 2022).

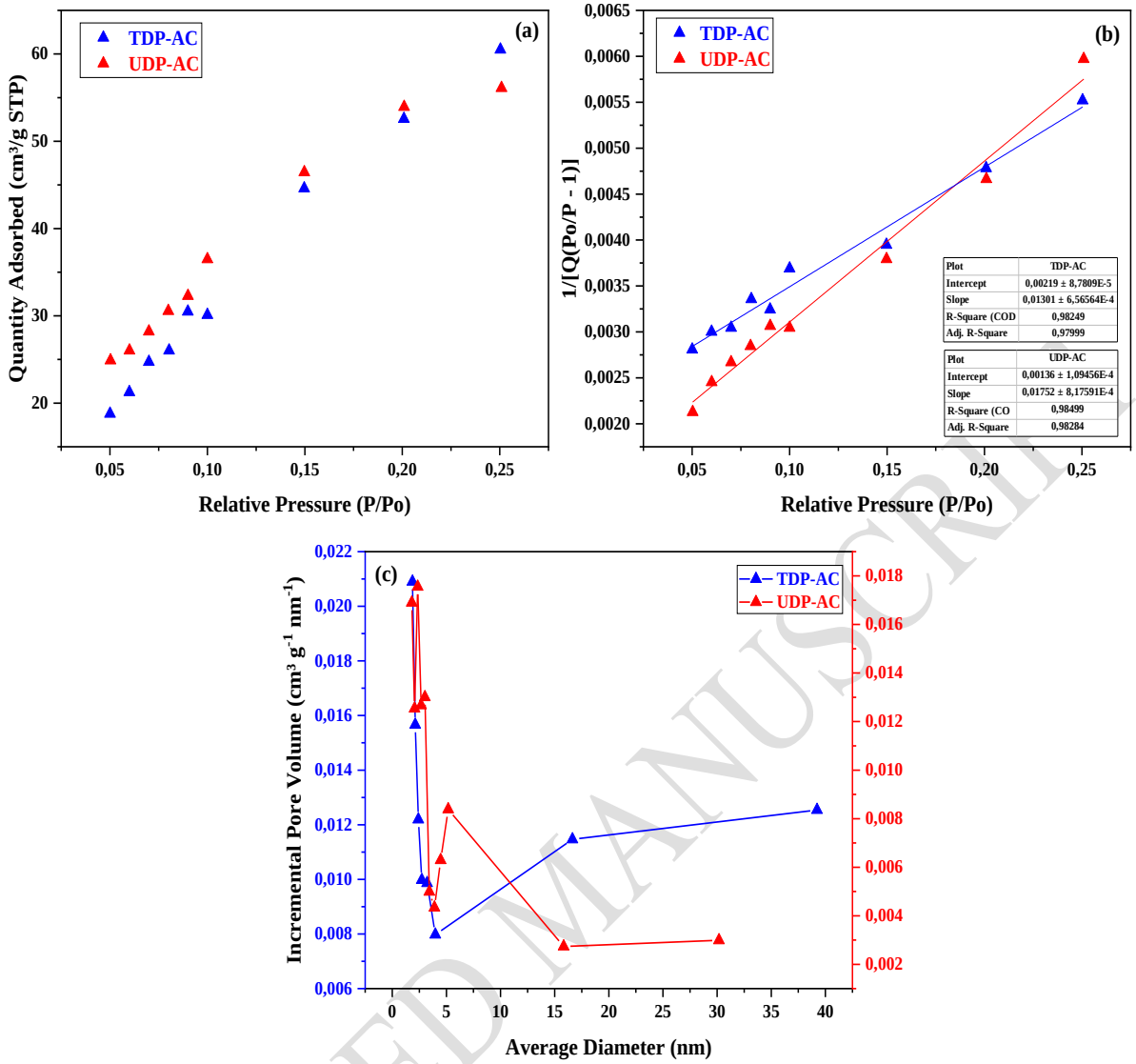

Figure 3. N_2 adsorption isotherm on TDP-AC and UDP-AC at 77 K (a), BET plot (b), Pore size distribution for TDP-AC and UDP-AC

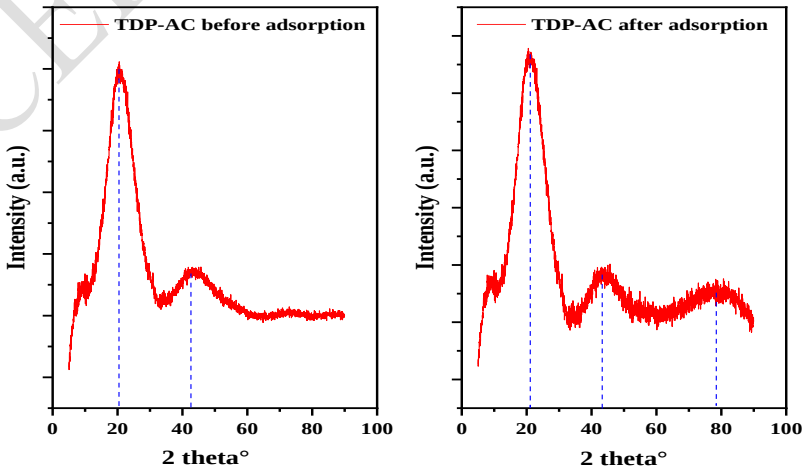

Figure 4. XRD patterns of TDP-AC before and after the adsorption of MB.

Figure 8 (a) and (b) show the SEM-EDX micrographs of TDP-AC and UDP-AC adsorbents, respectively. It is clear that the adsorbents surfaces possess heterogeneous and irregular rough surfaces with different porosity. As shown in Figure 8 (c) the detected sulfur (S) can be attributed to the role of H_2SO_4, which primarily contributed to the formation of sulfonic acid groups ($–SO_3$) on the TDP-AC surface. The presence of these sulfonic acid groups on the surface of TDP-AC will significantly enhance the negative charge of TDP-AC, making it more favorable for the adsorption of cationic dyes such as MB.

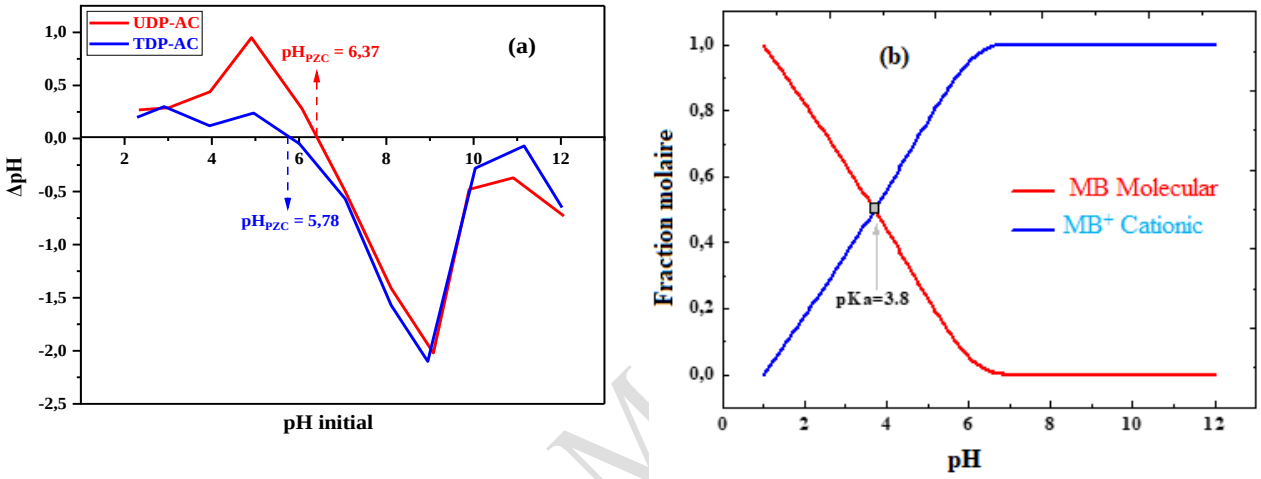

Figure 5. (a): Point of zero charge of UDP-AC and TDP-AC and (b): Speciation of MB dye.

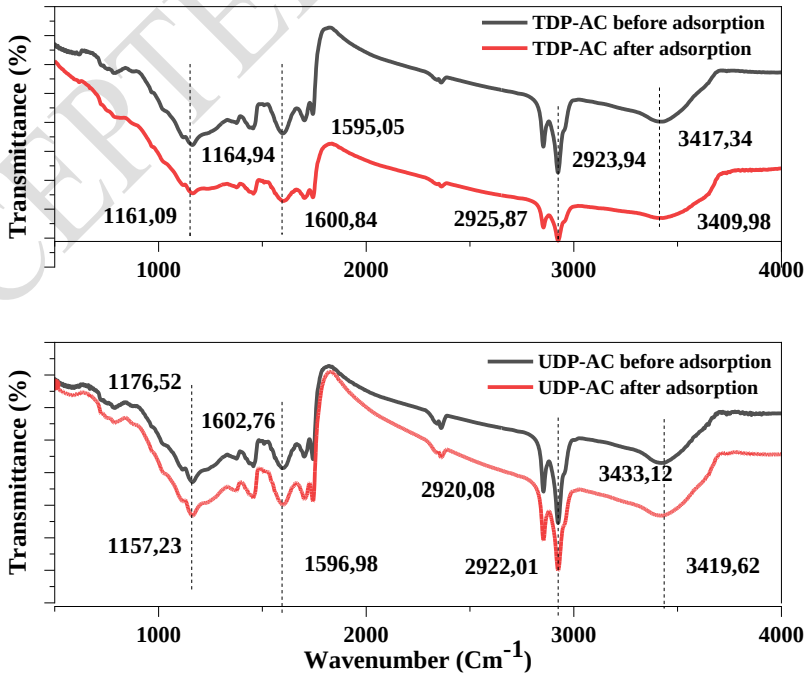

Figure 6. FTIR spectra of UDP-AC and TDP-AC before and after the adsorption of MB.

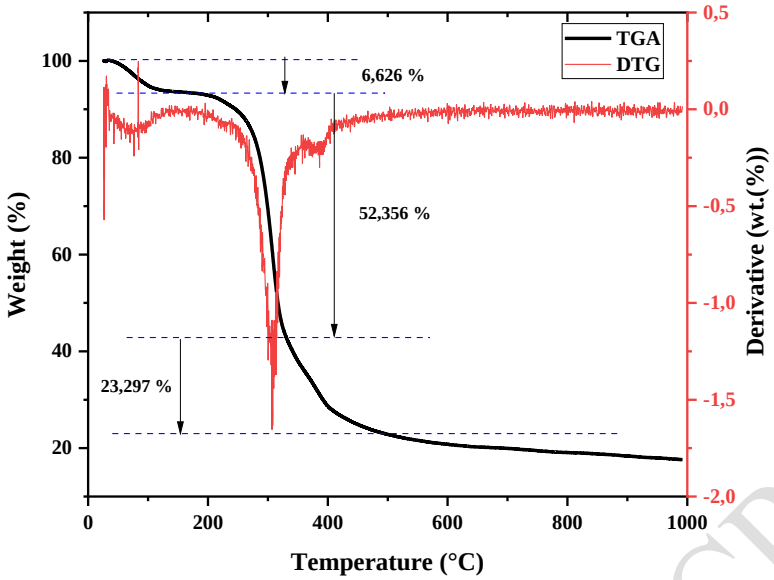

Figure 7. TGA/DGA curves of date pits.

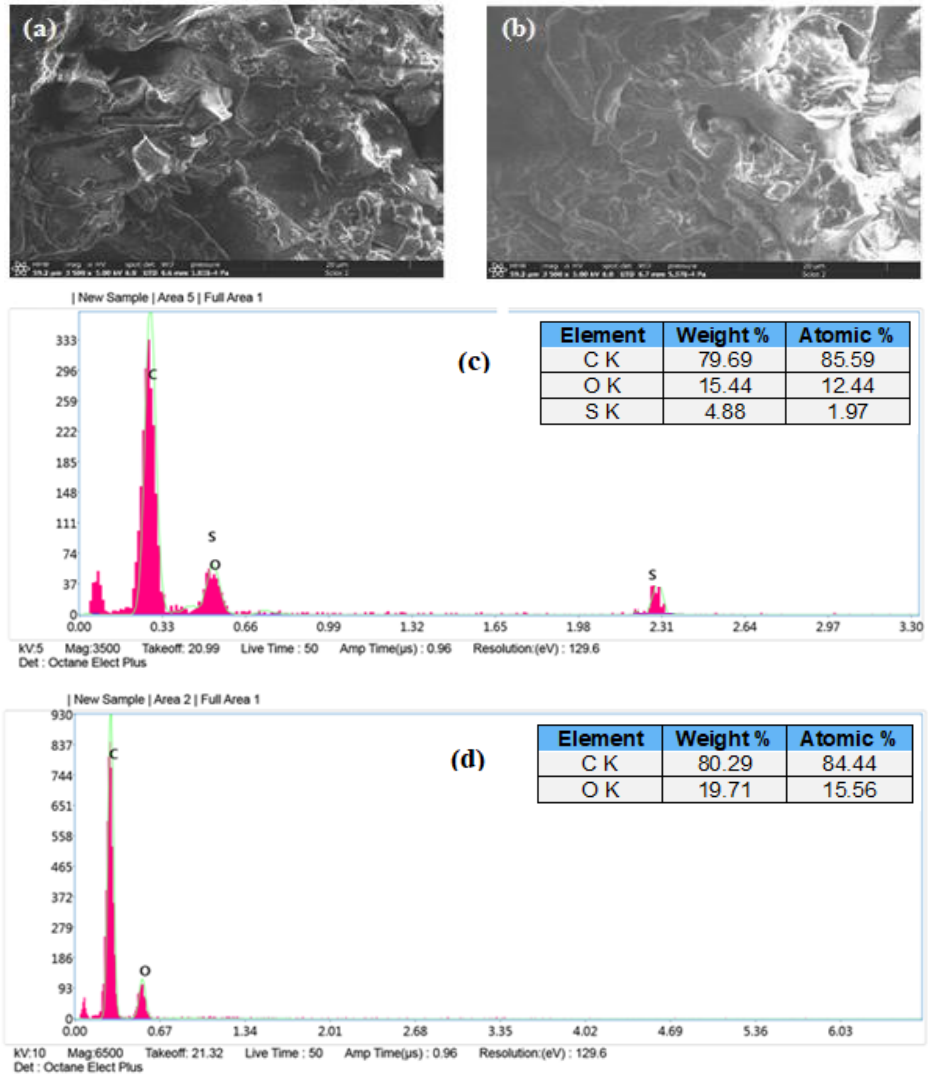

Figure 8. SEM images of TDP-AC (a) and UDP-AC (b), EDX graphs of TDP-AC (c) and UDP-AC (d).

3.2 Effect of adsorbent dosage

The adsorbent dosage plays a crucial role in the adsorption process. The selected range of adsorbent doses was 0.5 g L^{-1} to 5 g L^{-1}, with pH = 6 and an initial MB concentration of 100 mg L^{-1}. The results showed that the highest adsorption capacities were 166.69 mg g^{-1} and 186.48 mg g^{-1} for UDP-AC and TDP-AC, respectively, at an adsorbent dose of 0.5 g L^{-1} (Figure 9). However, the adsorption capacities q_e (mg g^{-1}) significantly decreased with increasing adsorbent dosage, reaching 16.08 mg g^{-1} and 15.10 mg g^{-1} for UDP-AC and TDP-AC, respectively. These results align with equation (2), which shows that adsorption capacity is inversely related to the adsorbent mass; as the adsorbent amount increases, the adsorbed quantity per unit mass decreases. Nevertheless, increasing the UDP-AC and TDP-AC dosages had no effect on the removal efficiency R (%), likely due to the increased availability of surface area and free binding sites for MB dye molecules. According to Figure 9, the optimal dosage for UDP-AC and TDP-AC is 0.5 g L^{-1}, which was used in the subsequent experiments (Kifuani et al., 2018).

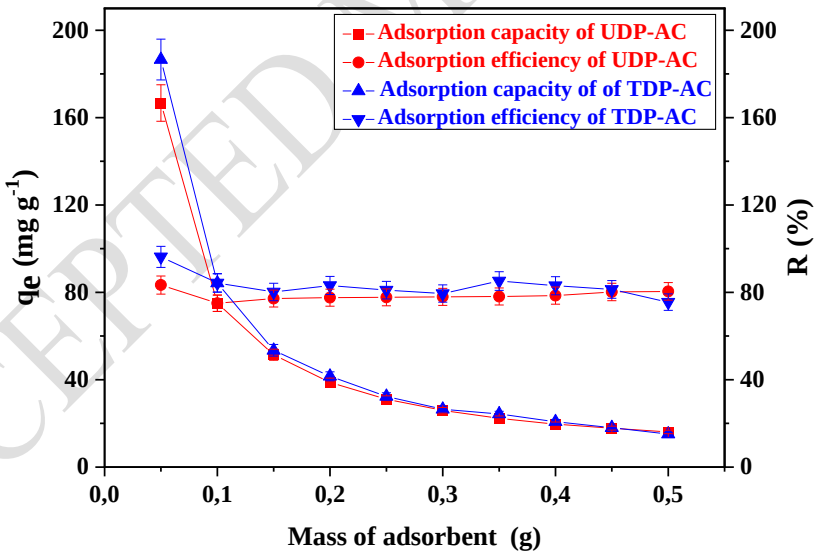

Figure 9. Effect of adsorbent dosage on adsorption of MB by UDP-AC and TDP-AC.

3.3 Effect of initial pH

The initial pH of the solution is a critical parameter in dye adsorption, as it influences the surface charge of the adsorbent, the ionization of acidic and basic functional groups, and the speciation of the adsorbate. Figure 10 illustrates the effect of initial pH on MB adsorption. As the initial pH increases

from 2 to 6, MB adsorption increases from 77.42 % and 88.64 % to 81.02% and 95.29% for UDP-AC and TDP-AC, respectively, after which no significant variation is observed. At low pH, MB^+ cations compete with H^+ ions for the active sites on UDP-AC and TDP-AC, limiting the adsorption efficiency. At pH values higher than the pH_{pzc} (6.37 for UDP-AC and 5.78 for TDP-AC), the surface of the adsorbents becomes negatively charged due to the dissociation of H^+ from oxygen-containing functional groups. This enhances MB^+ adsorption through electrostatic attraction between the cationic dye and the negatively charged adsorbent surface. Additionally, MB^+ molecules can interact with hydroxyl and carbonyl groups present on the adsorbent surfaces at higher pH values. Based on these findings, pH = 6 is considered the optimal pH for subsequent experiments. Figure 8 illustrates the possible adsorption mechanisms of MB onto TDP-AC (Hariharan et al., 2024) (Akköz & Coşkun, 2024) (Kuang et al., 2020) (Jawad et al., 2017).

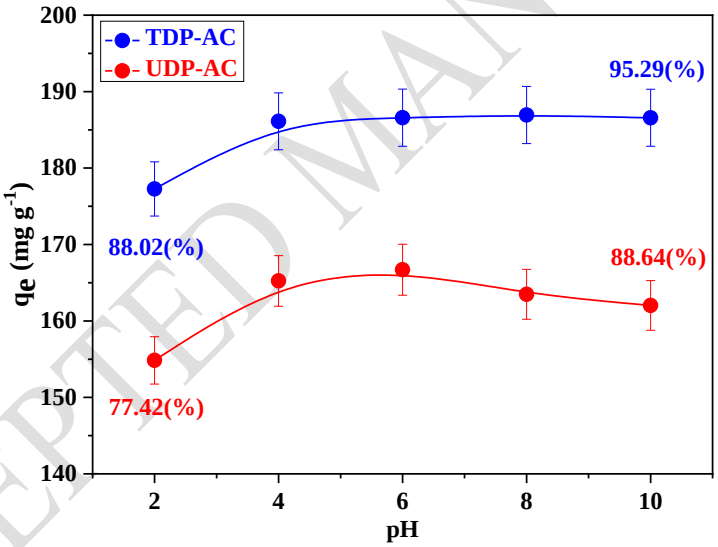

Figure 10. Effect of initial pH on MB adsorption capacity.

3.4 Effect of contact time

The estimation of contact time in water treatment is crucial for practical applications. As shown in Figure 11, the adsorption kinetic plots can be divided into two distinct phases. In the first phase (0 – 20 minutes), the adsorption capacity increases rapidly due to the abundance of vacant sites on the surfaces of UDP-AC and TDP-AC, as well as the strong electrostatic attraction between the cationic MB^+ dye and the negatively charged adsorbent surfaces (Wannawek et al., 2023). In the second phase,

after 20 minutes, the adsorption rate slows down as the number of available active sites decreases. Equilibrium is reached at approximately 120 minutes, corresponding to adsorption capacities of 154.94 mg g^{-1} for UDP-AC and 182.59 mg g^{-1} for TDP-AC. Beyond this point, no further increase in adsorption is observed, indicating the saturation of all active sites. Therefore, the optimal contact time for MB adsorption is determined to be 120 minutes.

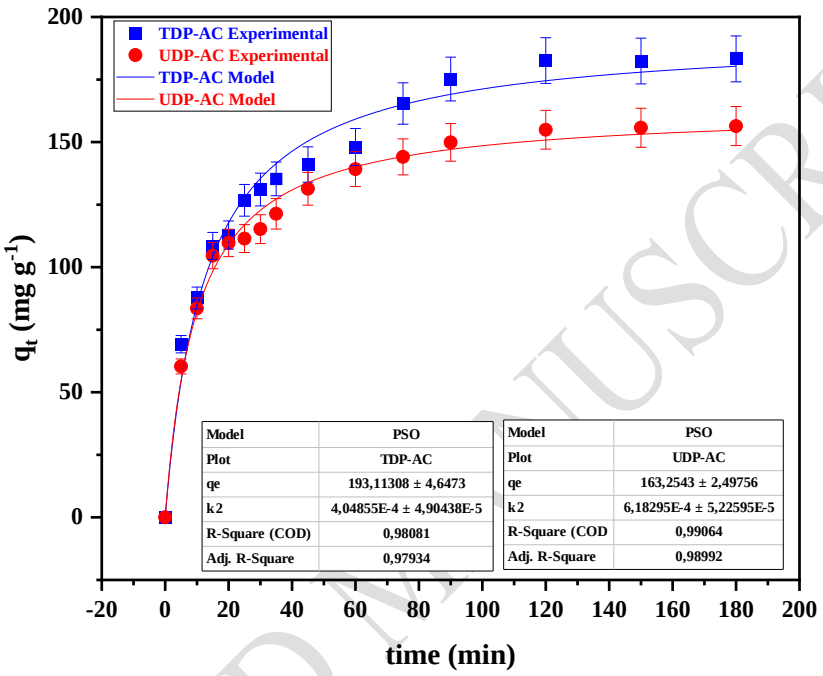

Figure 11. Effect of contact time on MB adsorption, Plots non-linear of PSO models for the adsorption of UDP-AC and TDP-AC. onto UDP-AC and TDP-AC.

3.5 Adsorption kinetic

Adsorption kinetics refers to the rate at which molecules or particles adhere to a surface and is often described by mathematical models that help to understand how adsorption occurs. Pseudo-first-order (PFO), pseudo-second-order (PSO) and intra-particle diffusion models (Figure 12 (a), (b) and (c)) were applied to understand the diffusion mechanism and rate controlling steps in adsorption phenomenon.

The linear forms of pseudo-first-order, pseudo-second-order and intra-particle diffusion models are given as follows, respectively (Gherbia et al., 2019) (Wannawek et al., 2023).

$$ln(q_e - q_t) = lnq_e - K_1 t \quad (4)$$

$$\frac{t}{q_t} = \frac{1}{K_2 q_e^2} + \frac{1}{q_e} \quad (5)$$

$$q_t = K_{id}\, t^{1/2} + C \quad (6)$$

Where k_1 (min^{-1}), k_2 (mg g^{-1} min^{-1}) and K_{id} (mg g^{-1} $min^{-1/2}$) are the rate constants of the pseudo-first-order, pseudo-second-order and intra-particle diffusion, respectively. q_t and q_e (mg g^{-1}) are the quantity of MB removed at time t (min) and at equilibrium, respectively. The constant C related to the thickness of the boundary.

The kinetic parameters presented in Table 1 show that the pseudo-second-order model provides a more accurate description of MB adsorption process on UDP-AC and TDP-AC, with high correlation coefficients R^2 values 0.997 for UDP-AC and 0.993 for TDP-AC respectively, compared to pseudo-first-order model R^2 0.975 for UDP and 0.946 for TDP. Further, a close agreement between the estimated adsorption capacity values (q_e, Cal = 166.66 and 188.80 mg g^{-1}) predicted by the pseudo-second-order model and the experimental values (q_e, Exp = 166.69 and 186.48 mg g^{-1}) for UDP-AC and TDP-AC, respectively.

The absence of straight lines passing through the origin as seen in the Figure 12 (c) indicates that pore diffusion alone does not control the rate of adsorption, suggesting a complex mechanism for the adsorption process, likely involving a combination of surface adsorption and intra-particle diffusion (Akköz & Coşkun, 2024) (M'sakni & Alsufyani, 2021) (Bayramoglu et al., 2009). The first step represents initial rapid adsorption which indicates the boundary layer effect where MB molecules are rapidly adsorbed onto the external surface of the activated carbon, in the second step, the slow and gradual increase in MB adsorption during this stage may indicate intra-particle diffusion, as the MB molecules penetrate the pores of the activated carbon. The flattening of the curve in the last steps indicates that the adsorption process is in equilibrium.

The kinetic study revealed that the PSO model provided the best fit for both TDP-AC and UDP-AC, as indicated by higher R^2 values. This suggests that the adsorption process is primarily controlled by chemisorption, involving electron sharing or exchange between the adsorbent and MB molecules (Ebelegi et al., 2020). In contrast, the PFO model showed a weaker correlation, indicating that

physisorption alone does not adequately describe the adsorption mechanism. These findings highlight the enhanced interaction between MB and the functionalized surface of TDP-AC, further confirming the impact of H_2SO_4 treatment in improving adsorption efficiency.

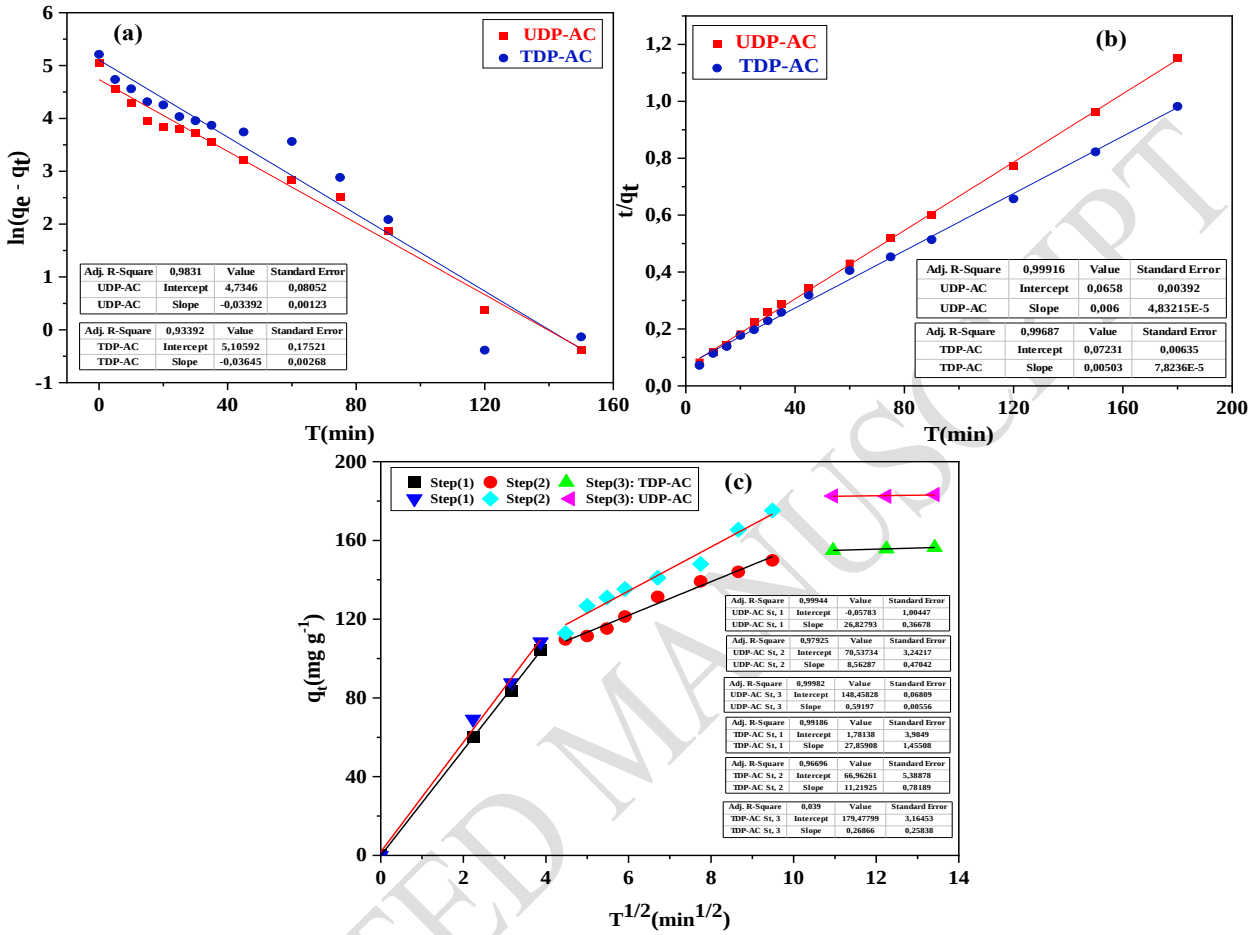

Figure 12. Pseudo-first-order (a), Pseudo-second-order (b) plots and intra-particle diffusion (c) plots of MB adsorption for UDP-AC and TDP-AC.

Table 1. Kinetic parameters for MB adsorption onto UDP-AC and TDP-AC.

	Pseudo-first-order				**Pseudo-second-order**		
Samples	$q_{e,Exp}$ (mg g^{-1})	$q_{e,Cal}$ (mg g^{-1})	k_1 (min^{-1})	R^2	$q_{e,Cal}$ (mg g^{-1})	k_2 (mg g^{-1} min^{-1})	R^2
UDP-AC	166.69	112.18	0.033	0.98	166.66	0.00054	0.99
TDP-AC	186.48	162.44	0.036	0.93	188.80	0.00034	0.99

	Intra-particle diffusion								
Samples	K_{id1} (mg g^{-1} $min^{-1/2}$)	C_1 (mg g^{-1})	R^2	K_{id2} (mg g^{-1} $min^{-1/2}$)	C_2 (mg g^{-1})	R^2	K_{id3} (mg g^{-1} $min^{-1/2}$)	C_3 (mg g^{-1})	R^2
UDP-AC	26.82	0.057	0.99	70.53	08.56	0.97	0.57	148.4	0.99
TDP-AC	27.82	01.78	0.99	66.90	11.21	0.96	0.26	179.4	0.99

3.6 Adsorption isotherm

Several theoretical models have been used to describe the relationship between the amount of adsorbate adsorbed and the equilibrium concentration of the adsorbate on the surface of the adsorbent at a constant temperature, including Langmuir, Freundlich and Temkin isotherms. In this study, the experimental data from the batch experiments were analyzed using Langmuir, Freundlich and Temkin isotherm models.

The linear form of Langmuir model is expressed as follows (Gherbia et al., 2019) (Wannawek et al., 2023).

$$\frac{C_e}{q_e} = \frac{1}{q_{max}\, K_L} + \frac{1}{q_m} C_e \tag{7}$$

Where, q_e(mg g^{-1}) is the equilibrium adsorption amount (mg g^{-1}), C_e is the equilibrium concentration of the adsorbate (mg L^{-1}), q_{max} (mg g^{-1}) represents the monolayer adsorption capacity, while k_L (L mg^{-1}) is related to the heat of adsorption. Figure 14 (a) illustrates the linear plot of C_e/q_e against C_e, with a slope of $1/q_{max}$ and an intercept of $1/ (q_{max}\, k_L)$. The essential characteristics of the Langmuir isotherm can be expressed using a dimensionless separation factor R_L, which is calculated as follows (Gherbia et al., 2019) (Wannawek et al., 2023).

$$R_L = \frac{1}{1+K_L C_0} \tag{8}$$

Where C_0 presents the initial adsorbate concentration (mg L^{-1}), K_L (L mg^{-1}) refers to the Langmuir constant and R_L is the separation factor is used to indicate the type of the isotherm, linear if (R_L= 1), irreversible when (R_L= 0), favorable if R_L in the range (0 to 1) and unfavorable when (R_L> 1).

The Freundlich isotherm model is expressed by the following equation (Gherbia et al., 2019) (Wannawek et al., 2023).

$$ln\, q_e = ln\, K_F + \frac{1}{n} C_e \tag{9}$$

Where, q_e represents the amount of adsorbate adsorbed at equilibrium (mg g^{-1}), C_e is the equilibrium concentration of the adsorbate in the solution (mg L^{-1}), K_F is the Freundlich constant related to adsorption capacity (mg g^{-1}) (L $mg^{-1})^{1/n}$, and (1/n) is related to the adsorption intensity and the favorability of the adsorption process. The Freundlich isotherm is often used when the adsorption is not limited to a monolayer and exhibits a heterogeneous surface.

The Temkin isotherm postulates that (n) the heat of adsorption for all molecules within the layer decreases linearly as coverage increases due to interactions between the adsorbent and adsorbate, and (nn) adsorption is defined by a uniform distribution of binding energies, up to a maximum binding energy, as expressed in the following equation (Kuang et al., 2020).

$$q_e = \frac{RT}{b_T} ln\, k_T + \frac{RT}{b_T} ln\, C_e \quad (10)$$

Where, b_T (kJ mol^{-1}) and k_T (L g^{-1}) are the Temkin constants, were calculated by analyzing the slope and intercept of the graphs generated from the relationship between q_e and ln C_e.

Figures 14 (a), (b) and (c) showed the plots of linear forms of Langmuir, Freundlich and Temkin isotherms, the parameters obtained from the applying both models are shown in Table 2, the results showed that the Langmuir model had the best fit compared to the Freundlich isotherm model, indicating that the adsorption on UDP-AC and TDP-AC is localized on a monolayer and homogeneous sites, with higher correlation coefficients (R^2> 0.99) and maximum adsorption capacities (q_{max}) were 270.27 and 327.86 (mg g^{-1}) at 25 °C for UDP-AC and TDP-AC, respectively. The adsorbent treated with H_2SO_4 presented the highest adsorption capacity compared to untreated activated carbon indicating that H_2SO_4 played a significant influence on MB adsorption process. It was also found that the values of the dimensionless separation factor R_L are 0.013 and 0.017 for UDP-AC and TDP-AC, respectively. This indicates that the adsorption of MB on UDP-AC and TDP-AC was favorable under the experimental conditions studied. TDP-AC exhibited a significantly higher R^2 than UDP-AC in the Temkin model. This can be attributed to the fact that the heat of adsorption of the molecules in the layer decreases linearly with surface coverage due to adsorbent-adsorbate interactions. Additionally, the adsorption process is characterized by a uniform distribution of binding energies up to the maximum binding energy (Sukla Baidya & Kumar, 2021).

Indicating that the adsorption of MB onto UDP-AC and TDP-AC, was favorable under the experimental conditions studied. The maximum adsorption capacities (q_{max}) of MB by UDP-AC and TDP-AC compared to other adsorbents mentioned in previous literatures are shown in Table 4.

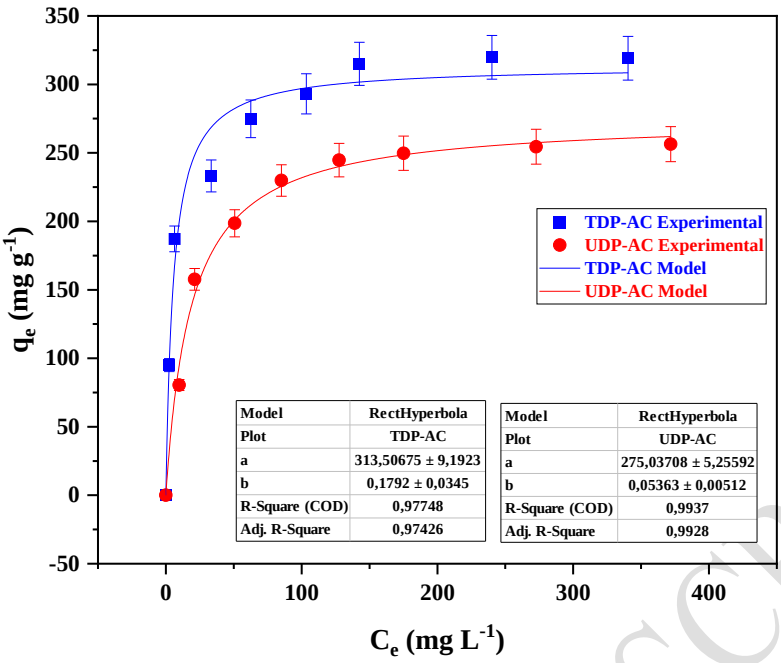

Figure 13. MB adsorption isotherms on UDP-AC and TDP-AC, Plot non-linear of Langmuir isotherm models for the adsorption of UDP-AC and TDP-AC.

The Langmuir isotherm's best fit indicates a uniform distribution of adsorption sites, where each site has identical activation energy and enthalpy, leading to a well-defined saturation point that enhances control in applications like water treatment (M. I. Khan et al., 2025).

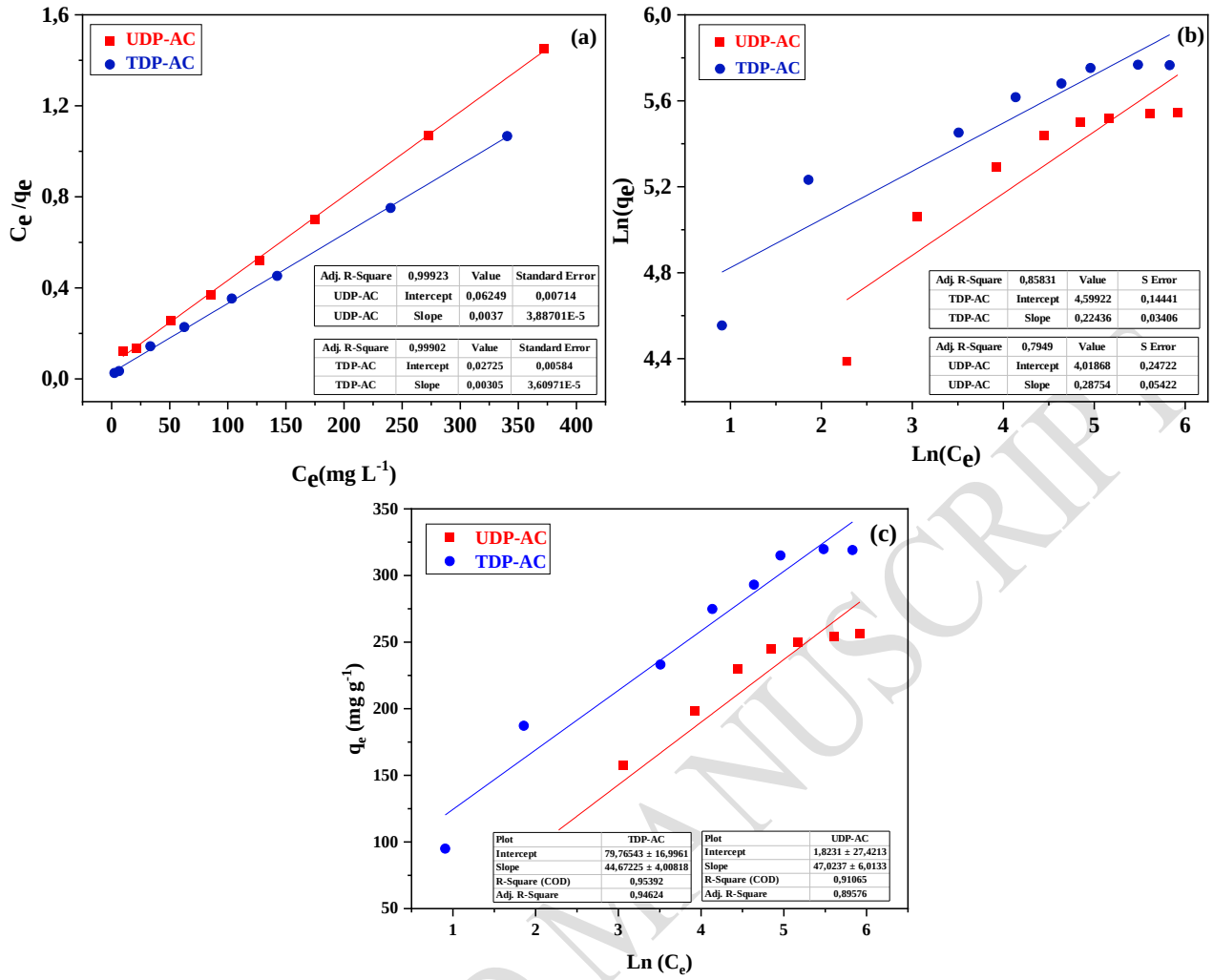

Figure 14. Plot of linear forms of Langmuir (a), Freundlich (b) and Temkin isotherm models for the adsorption of UDP-AC and TDP-AC.

Table 2. Isotherm parameters for MB adsorption onto UDP-AC and TDP-AC.

	Langmuir isotherm				**Freundlich isotherm**		
Adsorbents	q_{max} (mg g^{-1})	K_L (L mg^{-1})	R_L	R^2	K_F (mg g^{-1}) (L $mg^{-1})^{-n}$	n^{-1}	R^2
UDP-AC	270.27	0.148	0.013	0.999	54.94	0.287	0.794
TDP-AC	327.86	0.111	0.017	0.999	97.99	0.224	0.858
	Temkin isotherm						
Adsorbents	b_T (J mol^{-1})		k_T (L mg^{-1})		R^2		
UDP-AC	47.023		1.039		0.896		
TDP-AC	44.672		5.963		0.946		

3.7 Reusability studies

Despite the many advantages of adsorption, there are limitations in the use of adsorbents due to the saturation of the adsorbent with pollutants after adsorption process. Therefore, a large number of techniques are studying the possibility of regenerating adsorbents saturated with pollutants to avoid storing them or throwing them into nature, which leads to environmental problems. Several methods are used in the desorption process, such as using thermal, electrochemical and chemical regeneration

but desorption using the thermal process is expensive and produces byproducts that are harmful to the environment (Patel, 2021). Therefore, using acidic eluent is an easy, simple, effective process that does not take long.

The desorption process was studied after the adsorption experiment by batch technique, where the adsorbent particles saturated with MB were separated and then added to 100 mL of the hydrochloric acid solution HCl (0.1 M) was employed as eluting agent at 25°C, stirring at 250 rpm for 1h, after that, the adsorbent particles in the solution was separated using membrane (0.45 µm), and then the sample was rinsed with distilled water and dried at 100°C for reuse in another adsorption experiment. The MB concentration was analyzed using ultraviolet–visible spectroscopy (U-VIS) (model U-2000) at $\lambda = 664$ nm.

The figure 15 presents the removal efficiency of TDP-AC and UDP-AC, in the first cycle the removal efficiency were 88.15 and 81.73 (%) for TDP-AC and UDP-AC, respectively.

The removal efficiency decreased to 64.54 and 51.81(%) in the second cycle, 50. 26 and 42.98(%) in the third cycle to reach 42.10 and 33.17(%) in the fourth cycle for TDP-AC and UDP-AC, respectively. This result could be justified by the loss of performance the active sites on the surface of the adsorbents (Thiam et al., 2020). Therefore, both adsorbents TDP-AC and UDP-AC can be used for a limited number of adsorption/desorption cycles (Hazourli et al., 1996). Through desorption experiments, it can be concluded that the desorption of MB from UDP-AC and TDP-AC using HCl acid can be driven by the physical process as well as the chemical process. Regarding the physical process, it has been observed that quantities of MB are released rapidly once UDP-AC and TDP-AC come in contact with the HCl acid solution, this is mainly due to the adsorbed MB through the weakest type of bonds such as Van der Waals and hydrogen bonds, as for the chemical process, it results from the release of MB that was previously adsorbed by the functional groups present on the surface of UDP-AC and TDP-AC, where the process takes place through ion exchange between H_3O^+ and the MB molecules.

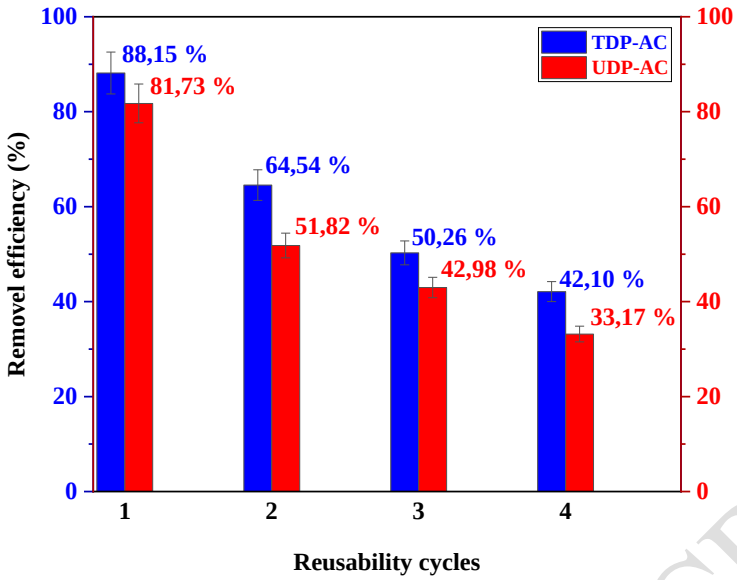

Figure 15 : Reusability of TDP-AC and UDP-AC for MB dye.

3.8 Thermodynamic studies

Thermodynamics of the adsorption process involves analyzing the thermodynamic parameters to understand the feasibility and spontaneity of the process by calculating the enthalpy change of adsorption ΔH°, entropy change ΔS°, and Gibbs enthalpy change values ΔG°. The values of ΔH°, ΔS° and ΔG° can be determined by the following equations (Ansari et al., 2016) (Mennas et al., 2023).

$$\Delta G° = \Delta H° - T\Delta S° \quad (11)$$

$$\Delta G° = -RT\, lnK_d° \quad (12)$$

$$lnK°_d = \frac{\Delta S°}{R} - \frac{\Delta H°}{RT} \quad (13)$$

$$K_d = \frac{q_e}{C_e} \quad (14)$$

Where, K_d is the distribution coefficient, T (K) is the temperature in Kalvin, R = 8.314 (J mol^{-1} K^{-1}) is the gas constant, q_e is the equilibrium quantity and C_e is the equilibrium concentration of MB solution.

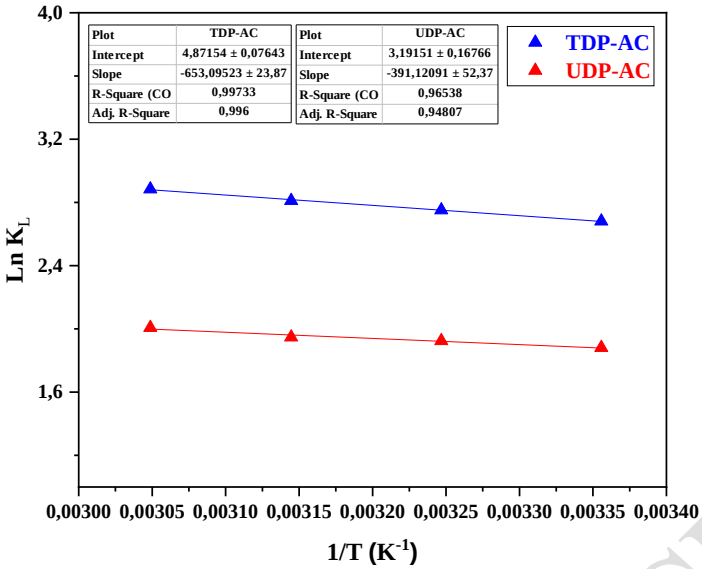

Figure 16. Van't Hoff plots for the adsorption of MB onto UDP-AC and TDP-AC.

Table 3. The thermodynamic characteristics for the adsorption of MB onto UDP-AC and TDP-AC.

Samples	Temperature (K)	UDP-AC	TDP-AC
ΔG° (kJ mol^{-1})	298	-4.660	-6.643
	308	-4.929	-7.047
	318	-5.148	-7.432
	328	-5.474	-7.865
ΔH° (kJ mol^{-1})		3.251	5.429
ΔS° (kJ K^{-1} mol^{-1})		0.0265	0.0405
R^2		0.948	0.996

The Figure 16 represents the Van't Hoff plots for the adsorption of MB onto UDP-AC and TDP-AC at different temperatures: 298, 308, 318 and 328 K. The results obtained are summarized in the Table 3. As shown in the Table 3, the values of Gibbs free energy change ΔG° are negative, indicating that the process is spontaneous and thermodynamically favorable on UDP-AC or TDP-AC. Also, when the temperature increased from 298 to 328 K, the values of free enthalpy change ΔG° decrease from (-4.660) to (-5.474 kJ mol^{-1}) and from (-6.643) to (-7.865 kJ mol^{-1}) for UDP-AC and TDP-AC, respectively, which indicates an increase in the spontaneous adsorption process, which leads to an increase in the adsorption capacity at high temperatures. The enthalpy changes of adsorption ΔH° is greater than zero, indicating that the adsorption process is endothermic, and lower values of ΔH°< 20 kJ mol^{-1} correspond to physisorption interactions. These low values confirm that the dominant interactions are weak non-covalent forces, such as van der Waals forces and electrostatic interactions,

rather than strong chemical bond formation as in chemisorption. ΔS is greater than zero, suggests an increase in randomness at the solid-liquid interface during adsorption. This can be attributed to the displacement of pre-adsorbed water molecules and the enhanced mobility of MB molecules on the adsorbent surface (Ebelegi et al., 2020) (Saha & Chowdhury, 2011) . Additionally, the porous nature of the activated carbon plays a significant role in facilitating adsorption by providing accessible sites for the adsorbate, contributing to the increase in entropy (Sen, 2023) (Wei et al., 2015).

Table 4. Comparison of adsorption capacities of MB dye on various adsorbents.

Adsorbent	**Activating agent**	**Rang MB concentration (mg L^{-1})**	**Contact time (min)**	**Adsorption capacity (mg g^{-1})**	**Reference**
UDP-AC	-	100	120	270.27	This work
TDP-AC	H_2SO_4	100	120	327.86	This work
Rumex abyssinicus plant	H_3PO_4	100	60	322	(Fito et al., 2023)
Biochar-derived date palm	-	20-200	360	206.61	(Zubair et al., 2020)
Pomegranate peels	H_2SO_4	200	420	212.7	(Genel et al., 2024)
Camellia sinensis L.	$ZnCl_2$	200	-	324.7	(Gao et al., 2013)
Terminalia catappa L	H_3PO_4	50	70	263.95	(Jabar et al., 2022)
Banana (Musa sapientum) peels	H_2SO_4	10-300	1440	250	(Jawad et al., 2018)
Phoenix dactylifera	NaOH	25-200	240	141.25	(Aldawsari et al., 2017)
Sugarcane juice	H_2SO_4	40	480	200	(Wannawek et al., 2023)
Lemongrass leaves	$C_6H_8O_7$	600	45	122.12	(Zein et al., 2023)
Commercial AC (CaliX post-carbon)	-	800	4320	286	(Mohd Nasir et al., 2021)
Commercial AC produced form coconut shell	KOH	100	120	45.9	(Yasin et al., 2007)

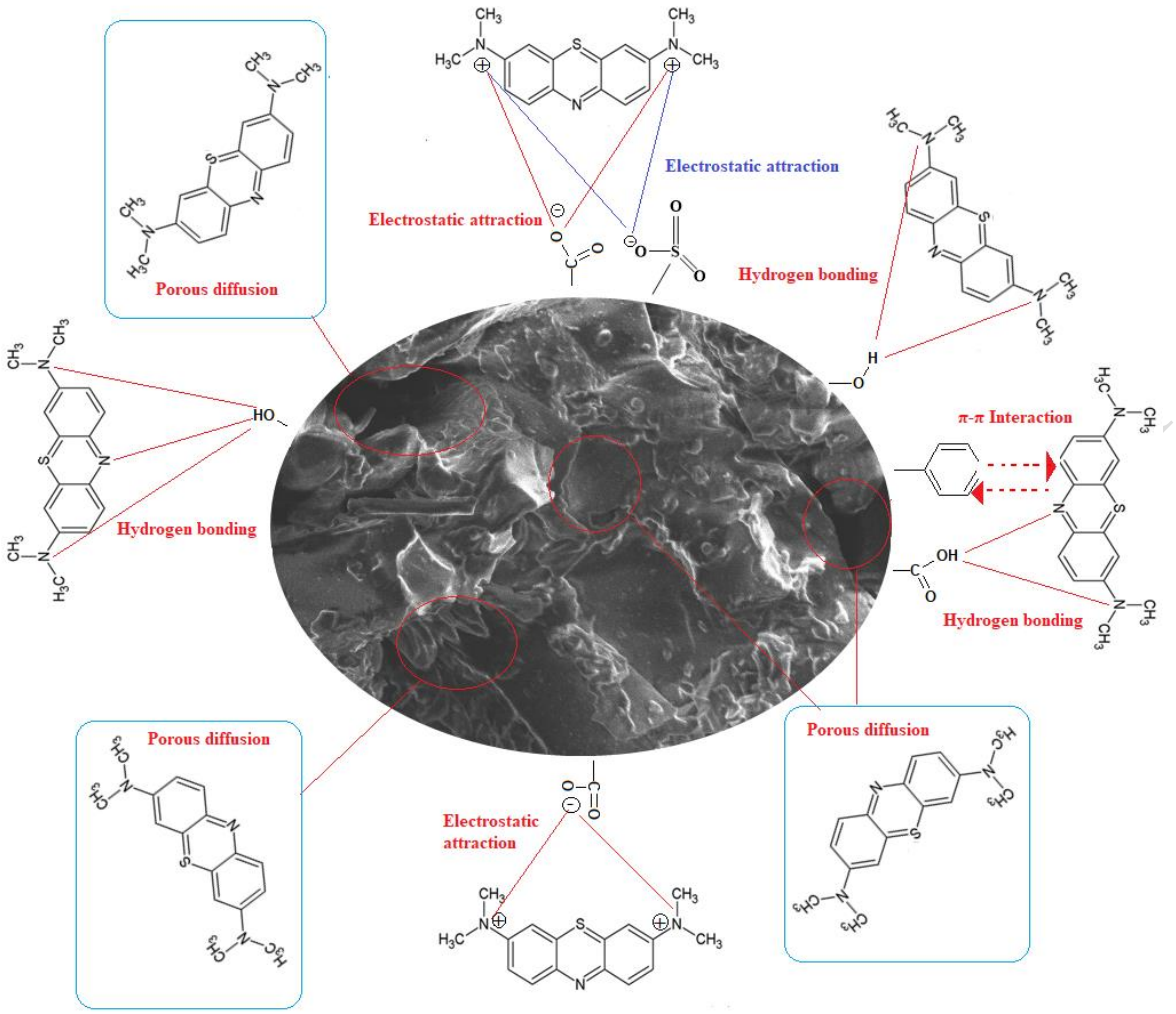

Figure 17. Possible mechanisms for MB adsorption onto TDP-AC.

3.9 Possible adsorption mechanism

The adsorption mechanism of methylene blue (MB) onto activated carbon (AC), whether chemically treated (TDP-AC) or untreated (UDP-AC), involves both physical and chemical interactions. As revealed by FT-IR analysis, AC contains various oxidizing (acidic) functional groups, which play a crucial role in the adsorption process. Electrostatic interactions between the cationic MB molecules and the negatively charged surface of the adsorbent are the primary driving forces. Additionally, secondary interactions, such as hydrogen bonding between donor and acceptor groups and π–π interactions between the π-electron system of AC and the aromatic ring structure of MB, further enhance adsorption. The process includes physisorption, governed by van der Waals forces and π–π interactions, as well as chemisorption, which involves hydrogen bonding and electrostatic attraction. Acid activation using H_2SO_4 significantly improves the adsorption efficiency of TDP-AC by

removing impurities, increasing surface acidity, and expanding the pore structure (Figure 17). These modifications facilitate the diffusion of dye molecules into the porous network and strengthen electrostatic attraction, making TDP-AC more effective than UDP-AC in MB removal (Bhatnagar et al., 2013) (Shen et al., 2008) (Togibasa et al., 2023).

4. Conclusion

The study demonstrated that H_2SO_4 activation significantly improved the adsorption capacity and removal efficiency of TDP-AC (327.86 mg g^{-1}, 95.29%) compared to UDP-AC (270.27 mg g^{-1}, 88.64%), due to an increase in surface area (286.36 m^2 g^{-1} vs. 230.3 m^2 g^{-1}) and enhanced physicochemical properties. Physically, H_2SO_4 expanded the pore structure, improving accessibility to adsorption sites, while chemically, it introduced functional groups (-SO_3H, -COOH, -OH) that enhanced electrostatic attraction and chemical bonding with MB. Adsorption followed the Langmuir model (R^2 = 0.99), indicating monolayer coverage, while kinetics were best described by the PSO model, suggesting a combination of physisorption (Van der Waals forces) and chemisorption (functional group interactions). Thermodynamic analysis confirmed that the process is spontaneous and endothermic, requiring low energy input. However, regeneration with HCl 0.1 M showed limited efficiency, highlighting the need for improved recovery methods.

Future research should focus on continuous adsorption processes, as they could offer greater efficiency than batch adsorption in practical applications. Additionally, while this study focused on synthetic MB solutions, investigating the performance of H_2SO_4-activated carbon in treating industrial effluents with complex pollutant mixtures is essential. Such studies would help assess its selectivity and efficiency under real-world conditions, ensuring its suitability for large-scale wastewater treatment. Overall, H_2SO_4-activated carbon derived from date pits represents a low-cost, energy-efficient, and environmentally friendly solution for wastewater treatment, with promising potential for industrial applications involving diverse contaminants.

References

Ahmad, A. A., Din, A. T. M., Yahaya, N. K. E., Khasri, A., & Ahmad, M. A. (2020). Adsorption of basic green 4 onto gasified Glyricidia sepium woodchip based activated carbon: Optimization, characterization, batch and column study. *Arabian Journal of Chemistry*, *13*(8), 6887–6903. https://doi.org/10.1016/j.arabjc.2020.07.002

Akköz, Y., & Coşkun, R. (2024). Cellulose- supported sulfated-magnetic biocomposite produced from hemp biomass: Effective removal of cationic dyes from aqueous solution. *International Journal of Biological Macromolecules*, *257*, 128747. https://doi.org/10.1016/J.IJBIOMAC.2023.128747

Al-Qodah, Z., & Shawabkah, R. (2009). Production and characterization of granular activated carbon from activated sludge. *Brazilian Journal of Chemical Engineering*, *26*(1). https://doi.org/10.1590/S0104-66322009000100012

Aldawsari, A., Khan, M. A., Hameed, B. H., AlOthman, Z. A., Siddiqui, M. R., Ahmed, A. Y. B. H., & Alsohaimi, I. H. (2017). Development of activated carbon from phoenix dactylifera fruit pits: Process optimization, characterization, and methylene blue adsorption. *Desalination and Water Treatment*, *62*, 273–281. https://doi.org/10.5004/dwt.2017.0529

Alghamdi, W. M., & El Mannoubi, I. (2021). Investigation of seeds and peels of citrullus colocynthis as efficient natural adsorbent for methylene blue dye. *Processes*, *9*(8). https://doi.org/10.3390/pr9081279

Ansari, S. A., Khan, F., & Ahmad, A. (2016). Cauliflower Leave, an Agricultural Waste Biomass Adsorbent, and Its Application for the Removal of MB Dye from Aqueous Solution: Equilibrium, Kinetics, and Thermodynamic Studies. *International Journal of Analytical Chemistry*, *2016*. https://doi.org/10.1155/2016/8252354

Bayramoglu, G., Altintas, B., & Arica, M. Y. (2009). Adsorption kinetics and thermodynamic parameters of cationic dyes from aqueous solutions by using a new strong cation-exchange resin. *Chemical Engineering Journal*, *152*(2–3), 339–346. https://doi.org/10.1016/j.cej.2009.04.051

Bhatnagar, A., Hogland, W., Marques, M., & Sillanpää, M. (2013). An overview of the modification methods of activated carbon for its water treatment applications. In *Chemical Engineering Journal* (Vol. 219, pp. 499–511). https://doi.org/10.1016/j.cej.2012.12.038

Bozbeyoglu, P., Duran, C., Baltaci, C., & Gundogdu, A. (2020). Adsorption Of Methylene Blue from Aqueous Solution with Sulfuric Acid Activated Corn Cobs: Equilibrium, Kinetics, and Thermodynamics Assessment. *Hittite Journal of Science & Engineering*, *7*(3), 239–256. https://doi.org/10.17350/HJSE19030000193

Chopra, I., & Singh, S. B. (2020). Kinetics and equilibrium study for adsorptive removal of cationic dye using agricultural waste- raw and modified cob husk. *International Journal of Environmental Analytical Chemistry*, *00*(00), 1–22. https://doi.org/10.1080/03067319.2020.1826458

Cox, M., El-Shafey, E., Pichugin, A. A., & Appleton, Q. (1999). Preparation and characterisation of a carbon adsorbent from flax shive by dehydration with sulfuric acid. *Journal of Chemical Technology and Biotechnology*, *74*(11). https://doi.org/10.1002/(sici)1097-4660(199911)74:11<1019::aid-jctb152>3.0.co;2-n

Ebelegi, A. N., Ayawei, N., & Wankasi, D. (2020). Interpretation of Adsorption Thermodynamics and Kinetics. *Open Journal of Physical Chemistry*, *10*(03), 166–182. https://doi.org/10.4236/ojpc.2020.103010

Edokpayi, J. N., Ndlovu, S. S., & Odiyo, J. O. (2019). Characterization of pulverized Marula seed husk and its potential for the sequestration of methylene blue from aqueous solution. *BMC Chemistry*, *13*(3), 1–14. https://doi.org/10.1186/s13065-019-0530-x

Fito, J., Abewaa, M., Mengistu, A., Angassa, K., Ambaye, A. D., Moyo, W., & Nkambule, T. (2023). Adsorption of methylene blue from textile industrial wastewater using activated carbon developed from Rumex abyssinicus plant. *Scientific Reports*, *13*(1), 1–17. https://doi.org/10.1038/s41598-023-32341-w

Gao, J. J., Qin, Y. B., Zhou, T., Cao, D. D., Xu, P., Hochstetter, D., & Wang, Y. F. (2013). Adsorption of methylene blue onto activated carbon produced from tea (Camellia sinensis L.) seed shells: Kinetics, equilibrium, and thermodynamics studies. *Journal of Zhejiang University: Science B*, *14*(7), 650–658. https://doi.org/10.1631/jzus.B12a0225

Genel, Y., Genel, İ., & Saka, C. (2024). Facile preparation of sulfonated carbon particles with pomegranate peels as adsorbent for enhanced methylene blue adsorption from aqueous solutions. *Biomass Conversion and Biorefinery*. https://doi.org/10.1007/s13399-024-05328-4

Gherbia, A., Chergui, A., Yeddou, A. R., Selatnia Ammar, S., & Boubekeur, N. (2019). Removal of methylene blue using activated carbon prepared from date stones activated with NaOH. *Global Nest Journal*, *21*(3), 374–380. https://doi.org/10.30955/gnj.002913

Harabi, S., Guiza, S., Álvarez-Montero, A., Gómez-Avilés, A., Bagané, M., Belver, C., & Bedia, J. (2024). Adsorption of Pesticides on Activated Carbons from Peach Stones. *Processes*, *12*(1). https://doi.org/10.3390/pr12010238

Hariharan, T., Gopi Raghunadh, P. V. S., Sivaramakrishnan, S., & Maguluri, L. P. (2024). Evaluation of aqueous phase adsorption of Acid Brown on mesoporous activated carbon prepared from Azolla Pinnate seaweed. *Global Nest Journal*, *26*(2). https://doi.org/10.30955/gnj.005560

Hazourli, S., Bonnecaze, G., & Astruc, M. (1996). Adsorption et electrosorption de composes organiques sur charbon actif en grains partie i - influence du potentiel imposé et du nombre de cycles adsorption and electrosorption of organic compounds on granular activated carbon part i - influence of applied potential and number of cycles. *Environmental Technology (United Kingdom)*, *17*(12). https://doi.org/10.1080/09593330.1996.9618457

Jabar, J. M., Odusote, Y. A., Ayinde, Y. T., & Yılmaz, M. (2022). African almond (Terminalia catappa L) leaves biochar prepared through pyrolysis using H3PO4 as chemical activator for sequestration of methylene blue dye. *Results in Engineering*, *14*. https://doi.org/10.1016/j.rineng.2022.100385

Jawad, A. H., Rashid, R. A., Ishak, M. A. M., & Ismail, K. (2018). Adsorptive removal of methylene blue by chemically treated cellulosic waste banana (Musa sapientum) peels. *Journal of Taibah University for Science*, *12*(6), 809–819. https://doi.org/10.1080/16583655.2018.1519893

Jawad, A. H., Sabar, S., Ishak, M. A. M., Wilson, L. D., Ahmad Norrahma, S. S., Talari, M. K., & Farhan, A. M. (2017). Microwave-assisted preparation of mesoporous-activated carbon from coconut (Cocos nucifera) leaf by H3PO4 activation for methylene blue adsorption. *Chemical Engineering Communications*, *204*(10), 1143–1156. https://doi.org/10.1080/00986445.2017.1347565

Khan, I., Saeed, K., Zekker, I., Zhang, B., Hendi, A. H., Ahmad, A., Ahmad, S., Zada, N., Ahmad, H., Shah, L. A., Shah, T., & Khan, I. (2022). Review on Methylene Blue: Its Properties, Uses, Toxicity and Photodegradation. In *Water (Switzerland)*. https://doi.org/10.3390/w14020242

Khan, M. I., Sufian, S., Hassan, F., Shamsuddin, R., & Farooq, M. (2025). Phosphoric acid based geopolymer foam-activated carbon composite for methylene blue adsorption: isotherm, kinetics, thermodynamics, and machine learning studies. *RSC Advances*, *15*(3), 1989–2010. https://doi.org/10.1039/D4RA05782A

Kifuani, K. M., Kifuani, A., Mayeko, K., Noki Vesituluta, P., Lopaka, B. I., & Bakambo, G. E. (2018). Adsorption of basic dye, Methylene Blue, in aqueous solution on bioadsorbent from agricultural waste of Cucumeropsis Naudin mannii. *Int. J. Biol. Chem. Sci*, *12*(1), 558–575.

Kuang, Y., Zhang, X., & Zhou, S. (2020). Adsorption of methylene blue in water onto activated carbon by surfactant modification. *Water (Switzerland)*, *12*(2). https://doi.org/10.3390/w12020587

Lu, Y. C., Kooh, M. R. R., Lim, L. B. L., & Priyantha, N. (2021). Effective and Simple NaOH-Modification Method to Remove Methyl Violet Dye via Ipomoea aquatica Roots. *Adsorption Science and Technology*, *2021*. https://doi.org/10.1155/2021/5932222

M'sakni, N. H., & Alsufyani, T. (2021). Removal of cationic organic dye from aqueous solution by

chemical and pyrolysis activated ulva lactuca. *Water (Switzerland)*, *13*(9). https://doi.org/10.3390/w13091154

Mechi, N., Ben Khemis, I., Dotto, G. L., Franco, D., Sellaoui, L., & Ben Lamine, A. (2019). Investigation of the adsorption mechanism of methylene blue (MB) on Cortaderia selloana flower spikes (FSs) and on Cortaderia selloana flower spikes derived carbon fibers (CFs). *Journal of Molecular Liquids*, *280*, 268–273. https://doi.org/10.1016/J.MOLLIQ.2019.02.024

Mennas, N., Lahreche, S., Chouli, F., Sabantina, L., & Benyoucef, A. (2023). Adsorption of Methylene Blue Dye by Cetyltrimethylammonium Bromide Intercalated Polyaniline-Functionalized Montmorillonite Clay Nanocomposite: Kinetics, Isotherms, and Mechanism Study. *Polymers*, *15*(17). https://doi.org/10.3390/polym15173518

Mohd Nasir, M. Z., Indiran, G., & Ahmad Zaini, M. A. (2021). Assessment of thermal regeneration of spent commercial activated carbon for methylene blue dye removal. *Particulate Science and Technology*, *39*(4), 504–510. https://doi.org/10.1080/02726351.2020.1775738

Mousavi, S. A., Shahbazi, D., Mahmoudi, A., & Darvishi, P. (2022). Methylene blue removal using prepared activated carbon from grape wood wastes: adsorption process analysis and modeling. *Water Quality Research Journal*, *57*(1), 1–19. https://doi.org/10.2166/wqrj.2021.015

Okoniewska, E. (2021). Removal of selected dyes on activated carbons. *Sustainability (Switzerland)*, *13*(8). https://doi.org/10.3390/su13084300

Olivares-Marín, M., Fernández-González, C., MacÍas-García, A., & Gómez-Serrano, V. (2012). Preparation of activated carbon from cherry stones by physical activation in air. Influence of the chemical carbonisation with H2SO4. *Journal of Analytical and Applied Pyrolysis*, *94*, 131–137. https://doi.org/10.1016/j.jaap.2011.11.019

Patel, H. (2021). Review on solvent desorption study from exhausted adsorbent. In *Journal of Saudi Chemical Society* (Vol. 25, Issue 8). Elsevier B.V. https://doi.org/10.1016/j.jscs.2021.101302

Pizzicato, B., Pacifico, S., Cayuela, D., Mijas, G., & Riba-Moliner, M. (2023). Advancements in Sustainable Natural Dyes for Textile Applications: A Review. In *Molecules* (Vol. 28, Issue 16). Multidisciplinary Digital Publishing Institute (MDPI). https://doi.org/10.3390/molecules28165954

Rafatullah, M., Sulaiman, O., Hashim, R., & Ahmad, A. (2010). Adsorption of methylene blue on low-cost adsorbents: A review. *Journal of Hazardous Materials*, *177*(1–3), 70–80. https://doi.org/10.1016/j.jhazmat.2009.12.047

Razali, N. S., Abdulhameed, A. S., Jawad, A. H., ALOthman, Z. A., Yousef, T. A., Al-Duaij, O. K., & Alsaiari, N. S. (2022). High-Surface-Area-Activated Carbon Derived from Mango Peels and Seeds Wastes via Microwave-Induced ZnCl2 Activation for Adsorption of Methylene Blue Dye Molecules: Statistical Optimization and Mechanism. *Molecules*, *27*(20). https://doi.org/10.3390/molecules27206947

Saha, P., & Chowdhury, S. (2011). Insight Into Adsorption Thermodynamics. In *Thermodynamics*. InTech. https://doi.org/10.5772/13474

Sarkar Phyllis, A. K., Tortora, G., & Johnson, I. (2022). Photodegradation. *The Fairchild Books Dictionary of Textiles*. https://doi.org/10.5040/9781501365072.12105

Sen, T. K. (2023). Adsorptive Removal of Dye (Methylene Blue) Organic Pollutant from Water by Pine Tree Leaf Biomass Adsorbent. *Processes*, *11*(7). https://doi.org/10.3390/pr11071877

Shen, W., Li, Z., & Liu, Y. (2008). Surface Chemical Functional Groups Modification of Porous Carbon. In *Recent Patents on Chemical Engineering* (Vol. 1).

Soltani, A., Faramarzi, M., & Parsa, S. A. M. (2021). A review on adsorbent parameters for removal of dye products from industrial wastewater. In *Water Quality Research Journal* (Vol. 56, Issue 4). https://doi.org/10.2166/wqrj.2021.023

Somsesta, N., Sricharoenchaikul, V., & Aht-Ong, D. (2020). Adsorption removal of methylene blue

onto activated carbon/cellulose biocomposite films: Equilibrium and kinetic studies. *Materials Chemistry and Physics*, *240*, 122221. https://doi.org/10.1016/J.MATCHEMPHYS.2019.122221

Sukla Baidya, K., & Kumar, U. (2021). Adsorption of brilliant green dye from aqueous solution onto chemically modified areca nut husk. *South African Journal of Chemical Engineering*, *35*, 33–43. https://doi.org/10.1016/j.sajce.2020.11.001

Thiam, A., Tanji, K., Assila, O., Zouheir, M., Haounati, R., Arrahli, A., Abeid, A., Lairini, S., Bouslamti, R., Zerouq, F., & Kherbeche, A. (2020). Valorization of Date Pits as an Effective Biosorbent for Remazol Brilliant Blue Adsorption from Aqueous Solution. *Journal of Chemistry*, *2020*. https://doi.org/10.1155/2020/4173152

Togibasa, O., Dahlan, K., Ansanay, Y. O., Runggaweri, A. F., & Merani, M. (2023). Surface modification of activated carbon from sago waste. *Journal of Metals, Materials and Minerals*, *33*(1), 95–100. https://doi.org/10.55713/jmmm.v33i1.1616

Tran, H. N., You, S. J., & Chao, H. P. (2017). Fast and efficient adsorption of methylene green 5 on activated carbon prepared from new chemical activation method. *Journal of Environmental Management*, *188*(2017), 322–336. https://doi.org/10.1016/j.jenvman.2016.12.003

Vojnović, B., Cetina, M., Franjković, P., & Sutlović, A. (2022). Influence of Initial pH Value on the Adsorption of Reactive Black 5 Dye on Powdered Activated Carbon: Kinetics, Mechanisms, and Thermodynamics. *Molecules*, *27*(4). https://doi.org/10.3390/molecules27041349

Wannawek, A., Keereeta, Y., Jansanthea, P., Panthuwat, W., Sassa-Deepaeng, T., & Pookmanee, P. (2023). Adsorption of methylene blue dye onto the natural liquid sugars-based carbon: Kinetic and thermodynamic. *Journal of Science and Agricultural Technology J. Sci. Agri. Technol*, *4*(2), 5–214. https://doi.org/10.14456/jsat.2023.8

Wei, W., Yang, L., Zhong, W. H., Li, S. Y., Cui, J., & Wei, Z. G. (2015). Fast removal of methylene blue from aqueous solution by adsorption onto poorly crystalline hydroxyapatite nanoparticles. *Digest Journal of Nanomaterials and Biostructures*, *10*(4), 1343–1363.

Wijaya, A., Siregar, P. M. S. B. N., Badri, A. F., Palapa, N. R., Amri, A., Ahmad, N., & Lesbani, A. (2023). Modified layered double hydroxide mg/m3+ (M3+ = al and cr) using metal oxide (cu) as adsorbent for methyl orange and methyl red dyes. *Periodica Polytechnica Chemical Engineering*, *67*(2). https://doi.org/10.3311/PPch.21608

Yasin, Y., Hussein, M. Z., & Ahmad, F. H. (2007). ADSORPTION OF METHYLENE BLUE ONTO TREATED ACTIVATED CARBON. In *The Malaysian Journal of Analytical Sciences* (Vol. 11, Issue 11).

Yeliz Ozudogru, & Ecem Tekne. (2023). Adsorption of Methylene Blue from Aqueous Solution Using Spent Coffee/Chitosan Composite. *Journal of Water Chemistry and Technology*, *45*(3), 234–245. https://doi.org/10.3103/s1063455x23030086

Zein, R., Satrio Purnomo, J., Ramadhani, P., Safni, Alif, M. F., & Putri, C. N. (2023). Enhancing sorption capacity of methylene blue dye using solid waste of lemongrass biosorbent by modification method. *Arabian Journal of Chemistry*, *16*(2). https://doi.org/10.1016/j.arabjc.2022.104480

Zubair, M., Mu'azu, N. D., Jarrah, N., Blaisi, N. I., Aziz, H. A., & A. Al-Harthi, M. (2020). Adsorption Behavior and Mechanism of Methylene Blue, Crystal Violet, Eriochrome Black T, and Methyl Orange Dyes onto Biochar-Derived Date Palm Fronds Waste Produced at Different Pyrolysis Conditions. *Water, Air, and Soil Pollution*, *231*(5). https://doi.org/10.1007/s11270-020-04595-x